

# NIR-Emitting Gold Nanoclusters–Modified Gelatin Nanoparticles as a Bioimaging Agent in Tissue

Nesma El-Sayed, Vanessa Trouillet, Anne Clasen, Gregor Jung, Klaus Hollemeyer, and Marc Schneider\*

Gold nanocluster (AuNC) synthesis using a well-distinguished polymer for nanoparticle-mediated drug delivery paves the way for developing efficient theranostics based on pharmaceutically accepted materials. Gelatin-stabilized AuNCs are synthesized and modified by glutathione for tuning the emission spectra. Addition of silver ions enhances the fluorescence, reaching also high quantum yield (26.7%). A simplified model can be proposed describing the nanoclusters' properties–structure relationship based on X-ray photoelectron spectroscopy data and synthesis sequence. Furthermore, these modifications improve fluorescence stability toward pH changes and enzymatic degradation, offering different AuNCs for various applications. The impact of nanocluster formation on gelatin structure integrity is investigated by Fourier transform infrared spectrometry and matrix-assisted laser desorption/ionization time of flight mass spectrometry, being important to further formulate gelatin nanoparticles (GNPs). The 218 nm-sized NPs show no cytotoxicity up to 600  $\mu\text{g mL}^{-1}$  and are imaged in skin, as a challenging autofluorescent tissue, by confocal microscopy, when transcutaneously delivered using dissolving microneedles. Linear unmixing allows simultaneous imaging of AuNCs–GNPs and skin with accurate signal separation. This underlines the great potential for bioimaging of this system to better understand nanomaterials' behavior in tissue. Additionally, it is drug delivery system also potentially serving as a theranostic system.


applications including bioimaging,<sup>[1–4]</sup> biolabeling,<sup>[5]</sup> sensing,<sup>[3,4,6,7]</sup> and therapy.<sup>[8]</sup> They are composed of several up to tens of gold atoms, giving rise to ultrasmall sized structures of less than 2 nm.<sup>[9]</sup> Due to their small size, they demonstrate molecule-like properties having discrete valence electronic states approaching the molecular orbitals.<sup>[10,11]</sup> They do not exhibit plasmon resonance as in case of larger gold nanoparticles but rather show fluorescence in the visible or the near-infrared (NIR) region.<sup>[12]</sup> Among their unique properties, having long lifetime NIR fluorescence, high two-photon excitation, and photostability alongside with biocompatibility<sup>[13]</sup> allow them to be attractive for imaging in tissue and in vivo.<sup>[2]</sup>

In addition to the quantum confinement effect, ligands play a fundamental role in controlling the chemical and physical properties of AuNCs.<sup>[14]</sup> Generally, nanoclusters form out of metal core–shell structure stabilized by ligands as staple-like motifs on the surface.<sup>[10]</sup> Tuning emission wavelength and intensity can be acquired by controlling the core size during synthesis.<sup>[15]</sup> In another scenario, charge transfer or electron donation from the ligands active groups to the metal core contributes as well in regulating the fluorescence properties.<sup>[16,17]</sup> Ligands can

## 1. Introduction

Gold nanoclusters (AuNCs) have gained growing interest recently, due to their unique properties and various potential

N. El-Sayed, Prof. M. Schneider  
Department of Pharmacy  
Biopharmaceutics and Pharmaceutical Technology  
Saarland University  
Campus C4 1, D-66123 Saarbrücken, Germany  
E-mail: Marc.Schneider@uni-saarland.de  
N. El-Sayed  
Department of Pharmaceutics  
Faculty of Pharmacy  
Alexandria University  
21521 Alexandria, Egypt

 The ORCID identification number(s) for the author(s) of this article can be found under <https://doi.org/10.1002/adhm.201900993>.

© 2019 The Authors. Published by WILEY-VCH Verlag GmbH & Co. KGaA, Weinheim. This is an open access article under the terms of the Creative Commons Attribution License, which permits use, distribution and reproduction in any medium, provided the original work is properly cited.

DOI: 10.1002/adhm.201900993

V. Trouillet  
Institute for Applied Materials (IAM) and Karlsruhe Nano Micro Facility (KNMF)  
Karlsruhe Institute of Technology (KIT)  
Hermann-von-Helmholtz-Platz 1  
76344 Eggenstein-Leopoldshafen, Germany  
A. Clasen, Prof. G. Jung  
Department of Biophysical Chemistry  
Saarland University  
Campus B2 2, D-66123 Saarbrücken, Germany  
Dr. K. Hollemeyer  
Physical Chemistry and Didactics of Chemistry  
Saarland University  
Campus B2 2, D-66123 Saarbrücken, Germany

stabilize the fluorescence of AuNCs against environmental conditions such as change of pH and temperature, etc.<sup>[18]</sup>

Proteins and peptides are attractive stabilizing, capping, and templating agents for AuNC synthesis. They offer mild reaction environment, water solubility, and biocompatibility which are all preferred attributes for the fabrication of metal nanoclusters.<sup>[19]</sup> Additionally, proteins possess biological, medicinal, and pharmaceutical applications. Glutathione has been extensively used for AuNC synthesis<sup>[4,20–24]</sup> due to the strong affinity of the thiol group to form Au–S bond.<sup>[23,25]</sup> Cysteine-containing proteins such as bovine serum albumin,<sup>[26–31]</sup> insulin,<sup>[32,33]</sup> trypsin,<sup>[34,35]</sup> and lysozyme<sup>[36,37]</sup> have been also explored for the same purpose. Other studies have also shown that basic amino acids together with tyrosine and tryptophan can contribute to the reduction of the ions to metallic gold.<sup>[38]</sup> Additionally, it has been reported that the protein organizational structure is controlling the NCs' properties, where amyloid fibril (cross- $\beta$ -sheet structures) formation can lead to redshift in fluorescence.<sup>[39]</sup>

However, the mechanism of nanocluster formation is still not fully understood. Careful selection of the suitable ligand for optimizing and stabilizing the optical properties of the nanoclusters is a prerequisite. On the other hand, correlating the physicochemical properties of AuNCs to their structure is very crucial. It is a step toward better understanding and easier properties manipulation to fulfill different applications. X-ray photoelectron spectroscopy (XPS) can act as a useful tool

to investigate the effect of ligands on the atomic structure of AuNCs by studying the oxidation state of the clusters forming elements and the binding properties.<sup>[10,27]</sup>

Synthesis of AuNC-labeled pharmaceutical proteins and polymers will pave the way and allow to obtain multifunctional nanoparticles (NPs) for simultaneous drug delivery and bioimaging and/or biosensing. Gelatin represents a promising carrier that has been widely used for the delivery of biomacromolecules and hydrophilic drugs<sup>[40]</sup> due to its hydrophilicity, biodegradability, and biocompatibility. The biocompatibility of the multifunctional NPs is essential; where AuNCs are easily excreted from the body due to their small size, less than the renal clearance cutoff, and gelatin NPs will degrade and solubilize. Up to our knowledge, gelatin has not been investigated yet for synthesis of fluorescent AuNCs, despite its widespread use in preparation of gold nanoparticles. We envisage that the gelatin-mediated synthesis of AuNCs might open the door for various pharmaceutical or biomedical applications. In this regard, we have succeeded to synthesis NIR-emitting AuNCs using gelatin. By varying the reaction conditions, we have managed to control the fluorescence properties of the resulting nanoclusters. AuNC-modified gelatin has proved to be capable of forming nanocarriers (gelatin nanoparticles (GNPs)) with the ultimate goal of imaging in tissue. Such system can be of high potential for theranostics for simultaneous bioimaging and delivery of macromolecules such as antigens.

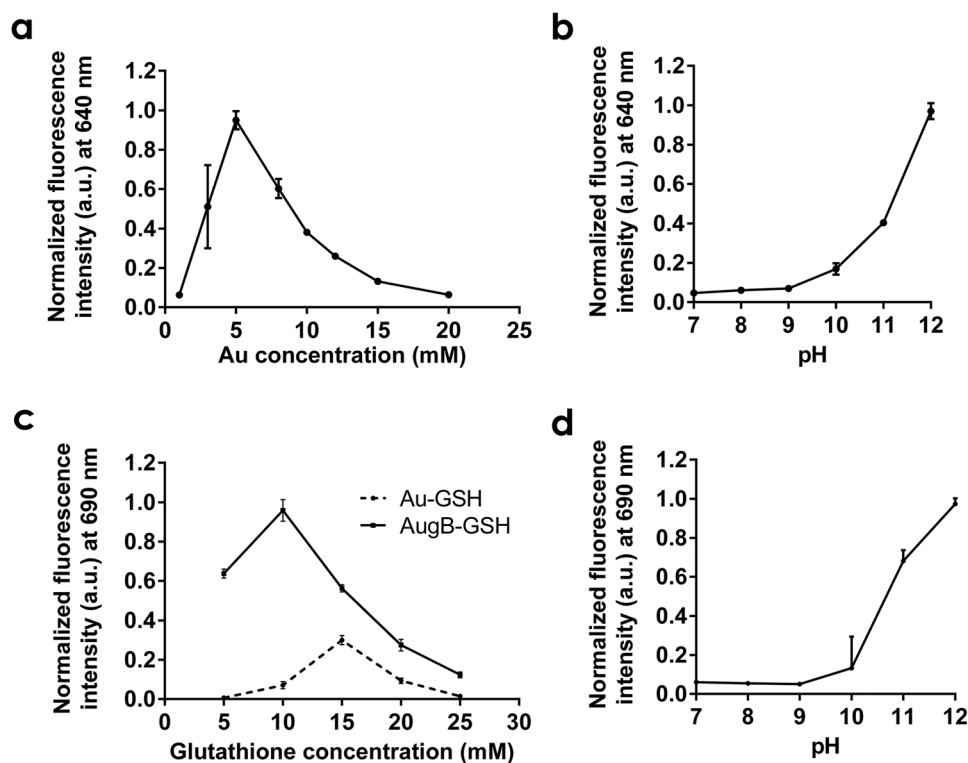


**Figure 1.** Gold nanoclusters stabilized by gelatin only; a) Effect of gold molar concentration and b) effect of pH on the maximum fluorescence emission at 640 nm. Gold nanoclusters stabilized by gelatin and glutathione (GSH); c) Effect of GSH concentration on the fluorescence of AuNCs at 690 nm, when used alone (Au–GSH) and in combination with gelatin (AuB–GSH) and d) effect of pH on the maximum fluorescence emission of the gelatin–GSH-stabilized AuNCs at 690 nm AuB–GSH: describes nanoclusters stabilized only using gelatin B and different concentrations of glutathione. Au–GSH: is the nano cluster stabilized with different concentrations of glutathione only without using gelatin.

## 2. Results and Discussion

### 2.1. Synthesis of Gelatin-Stabilized AuNCs

Gelatin is a natural polymer consisting of a mixture of proteins and polypeptides that result from the hydrolysis of collagen. We have utilized gelatin type B to sequester and reduce Au (III) to Au (0) that combine together to form AuNCs emitting fluorescence at  $\lambda_{\text{max}}$  640 nm. For optimizing the synthesis process, different gold concentrations and pH values have been tested. The fluorescence intensity directly rises with Au concentration up to  $5 \times 10^{-3}$  M, while further increase in concentration resulted in a gradual loss of fluorescence (Figure 1a and Figure S1 (Supporting Information)). The latter effect is due to the formation of larger gold nanoparticles that influence the fluorescence negatively by quenching.<sup>[41]</sup> At a concentration of  $30 \times 10^{-3}$  M gold chloride, only gold nanoparticles have been produced as observed by transmission electron microscopy (TEM) (Figure S2a, Supporting Information). On the other hand, adjusting the pH was crucial to initiate the reaction between gold and gelatin. At pH range (7–12), the fluorescence increased with pH to be maximized at pH 12 (Figure 1b). Among the amino acids composition of gelatin, the basic amino acids; arginine (8%)<sup>[42]</sup> and lysine (4%)<sup>[42]</sup> can reduce Au (III) ions to Au (0) by electron transfer from the side chain amines. According to Xu et al., arginine and lysine can form complexes with Au<sup>3+</sup> that can be further reduced by tyrosine under alkaline conditions,<sup>[38]</sup> however tyrosine represents only <0.5% of gelatin weight.<sup>[42]</sup> On the other hand, glutamic acid (10%)<sup>[42]</sup> can contribute to the thermal reduction of gold ions.<sup>[43]</sup> All these mechanisms can be contributing variably to the formation of AuNCs.

The polymer backbone structure and viscosity play a role in controlling the growth rate and the stabilization of AuNCs. In this regard, gelatin B showed better efficiency to form fluorescent AuNCs compared to gelatin A (Figure S3a, Supporting Information). This can be attributed to the glutamic acid content of gelatin B which results from the alkaline hydrolysis of collagen.<sup>[44]</sup> Additionally, more free amines are expected in gelatin B due to the lower isoelectric point (4–6) compared to 7–9 in gelatin A.<sup>[45]</sup> On the other hand, gelatin B of higher bloom (225 g) resulted in less fluorescence compared to bloom 75 g (Figure S3b, Supporting Information), which might be due to the higher flexibility of short polymer chains to interact with gold ions. Although the viscosity contributes to the AuNC stability, the excessively increased viscosity can possibly reduce the electron transfer to Au ions, resulting in lower reduction rate.<sup>[46]</sup> For upscaling the AuNC production, multiples of gelatin concentrations have been tested while multiplying the Au concentration to keep the ratio unchanged (Figure S4, Supporting Information).

Glutathione (GSH) is a strong reducing agent that has been widely used for the preparation of AuNCs due to the presence of thiol group (–SH). One-pot synthesis of AuNCs using gelatin and different concentrations of

glutathione allowed tuning the emission spectrum of the nano-clusters (Figure S5, Supporting Information). Selected GSH concentration of  $10 \times 10^{-3}$  M resulted in 50 nm redshift in the AuNC fluorescence ( $\lambda_{\text{em}} = 690$  nm). Interestingly, GSH alone, with the same concentration and under the tested reaction conditions, resulted in negligible fluorescence. Only GSH of concentration of  $15 \times 10^{-3}$  M resulted in detectable fluorescence when reacted with gold chloride that has been even enhanced by gelatin addition (Figure 1c). This proves the synergistic contribution of gelatin and GSH to form AuNCs. Ligand modification and so the introduction of more electron-rich functional groups can manipulate the electron transfer to the metal core, and thus influence the fluorescent properties of AuNCs.<sup>[16]</sup> Additionally, increasing the pH from 7 to 12 resulted in gradual increase in the fluorescence (Figure 1d).

### 2.2. Structure Integrity of Gelatin during AuNC Formation

A compromise between the AuNC formation and maintaining gelatin's integrity is necessary to further use the polymer for pharmaceutical purposes. Controlling the pH has the competence to manipulate the reaction rate (Figure 2a). Simultaneously, it affects the gelatin structure, especially at high temperature. At pH 12, after 6 h of the reaction with gold ions, gelatin has lost its gelling properties when cooled to 4 °C. By contrast, pH 11 preserves the gelation properties of the polymer till completion of the reaction at 24 h (Figure S6, Supporting Information). For further investigations about the gelatin structure, ninhydrin test has been performed to quantify the free amine groups over different time intervals of the interaction with gold. After 1 h of reaction at pH 12, the free amino groups have been reduced to 87% and this can be attributed to the coordination established between –NH<sub>2</sub> and Au. Then, the % increased to 94 after 3 h, continuing gradually to reach 145% after 24 h of the reaction, indicating gelatin degradation and hence the increase of free amine groups of the polypeptide (Figure 2b).

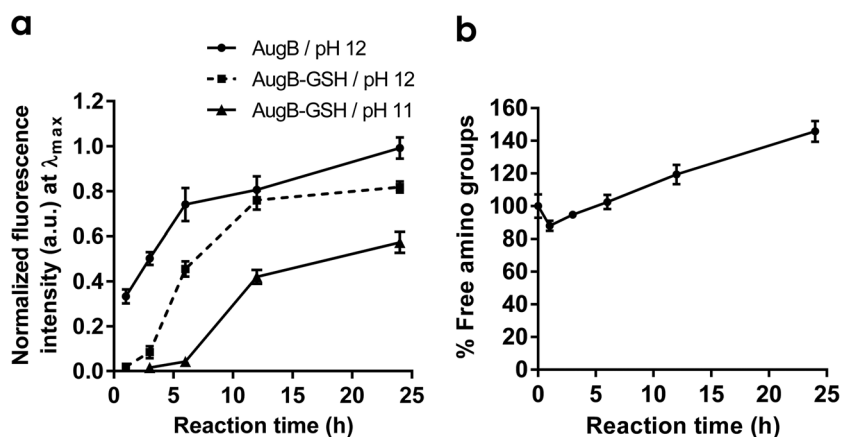


**Figure 2.** a) Effect of GSH addition and change of pH on the reaction rate for the formation of gelatin-stabilized AuNCs; represented by fluorescence intensity. The different tested reaction conditions are; 4% w/v gelatin at pH 12 (AugB/pH 12), 4% w/v gelatin and  $10 \times 10^{-3}$  M GSH at pH 12 (AugB–GSH/pH 12), and 4% w/v gelatin and  $10 \times 10^{-3}$  M GSH at pH 11 (AugB–GSH/pH 11). b) Quantification of the free amine groups of gelatin after different reaction times with gold chloride at pH 12 (AugB/pH 12) using ninhydrin test. AugB represents nanoclusters stabilized by gelatin B at different pH and reaction times.

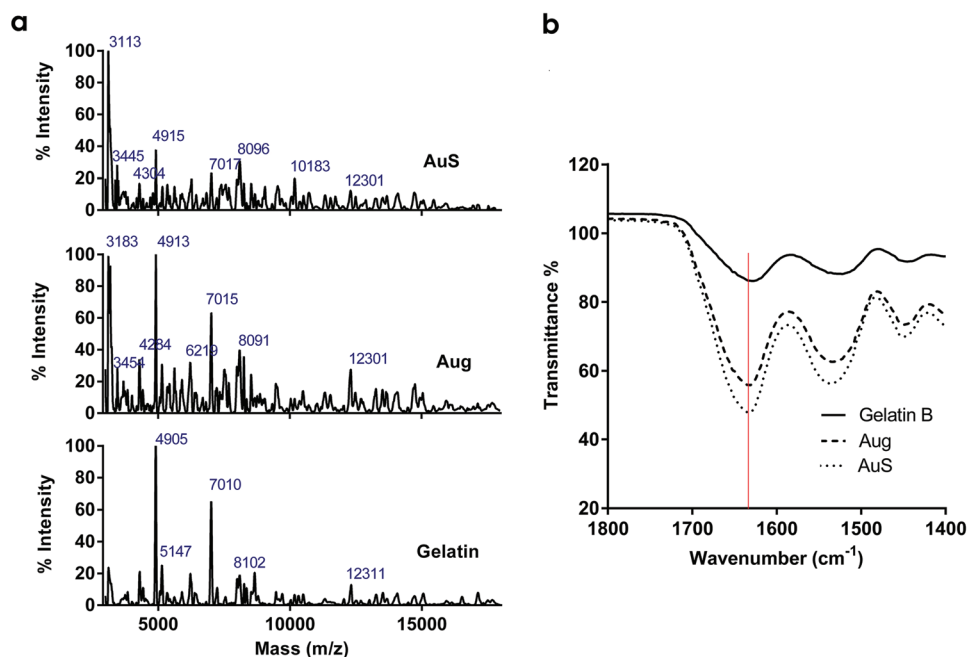


**Figure 3.** Investigating the effect of AuNC formation on the gelatin structure by comparing AuS and Aug to untreated gelatin. a) MALDI-TOF MS spectra recorded in positive mode show areas of similar mass ( $m/z$ ). b) FT-IR spectra showed a negligible shift in amide I from  $1629\text{ cm}^{-1}$  for gelatin to  $1632\text{ cm}^{-1}$  in both Aug and AuS, indicating  $\beta$ -sheets secondary structure ( $1623\text{--}1641\text{ cm}^{-1}$ ) for all of them. Aug is the optimized formulation of gelatin-stabilized nanoclusters with reaction time of 3 h and pH 12. AuS: represents the optimized formulation using gelatin and glutathione with reaction time of 24 h and pH 11.

Two AuNC formulations have been selected, so far, for further studies: AuNCs synthesized by gelatin at pH 12 and 3 h of reaction (Aug) and the other prepared by gelatin and GSH at pH 11 after 24 h reaction (AuS) (Table S1, Supporting Information). These formulations showed well detectable fluorescence by confocal microscopy upon excitation at 405 nm (Figure S7b, Supporting Information). They have been examined as well by Fourier transform infrared spectrometry (FT-IR) and matrix-assisted laser desorption/ionization time of flight mass spectrometry (MALDI-TOF MS) to reveal the changes in gelatin structure in comparison to the untreated polymer. MALDI-TOF MS is a common tool to study the core size of AuNCs and ligand composition. However, calculating the AuNC core size by detecting the number of gold atoms in such a case was not an accessible option due to the heterogeneous mass of the gelatin polypeptides mixture, in addition to the possible fragmentation of the nanoclusters during ionization.<sup>[27,47]</sup> In parallel, the examination of the change in the mass spectrum of gelatin could be determined. **Figure 3a** shows the mass spectra of gelatin and both nanocluster formulations: Aug and AuS. Peaks of lower molecular weight ( $m/z \approx 3100$ ) appear in both Aug and AuS. The two spectra show other regions of almost similar  $m/z$  ratio compared to untreated gelatin, with variable peak intensities. Using the specified conditions for Aug and AuS synthesis controlled gelatin degradation while maintaining the gelling properties as has been observed earlier (Figure S6, Supporting Information).

On the other hand, FT-IR is used commonly to investigate the conformational changes of proteins and peptides, especially in the secondary structure. Amide I ( $1600\text{--}1700\text{ cm}^{-1}$ , mainly due to CO stretching vibration) and amide II ( $\approx 1550\text{ cm}^{-1}$ , NH

bending and CN stretching vibrations) are characteristic bands for the secondary structure. However, correlating the secondary structure to amide II is less straightforward than amide I.<sup>[48]</sup> Untreated gelatin showed amide I band at  $1629\text{ cm}^{-1}$  (Figure 3b), revealing  $\beta$ -sheets' secondary structure (indicated by amide I in the range  $1623\text{--}1641\text{ cm}^{-1}$ ).<sup>[48]</sup> A very small shift to  $1632\text{ cm}^{-1}$  after the reaction with gold (in Aug and AuS) indicates no or minimal changes in the secondary structure. By controlling the pH along with the reaction time, we managed to maintain the structural and conformational integrity of the gelatin, to be further utilized for NP fabrication.

### 2.3. Fluorescence Enhancement

Enhancing the fluorescence will be crucial for various bioimaging purposes, especially in tissues. One strategy for improving the fluorescence intensity is the formation of alloy nanoclusters, by the doping of another noble metal during the nanoclusters growth. Silver and gold has been considered as a common combination for fabrication of alloy nanoclusters.<sup>[49,50]</sup> Modification of gold nanoclusters by silver has been reported to enhance the emission.<sup>[49,51]</sup> By using gelatin and GSH as ligands, it was important to optimize the Ag: Au molar ratio (0.4) to obtain the highest possible fluorescence intensity (Figure S8, Supporting Information). Surprisingly, doping Ag ions after 6 h from the start of the reaction resulted in 2.5-fold increase in fluorescence rather than addition at the start of the reaction (Figure S8, Supporting Information). This might indicate the significance of the different noble metal atoms arrangement in the core for controlling the fluorescence properties of the alloy

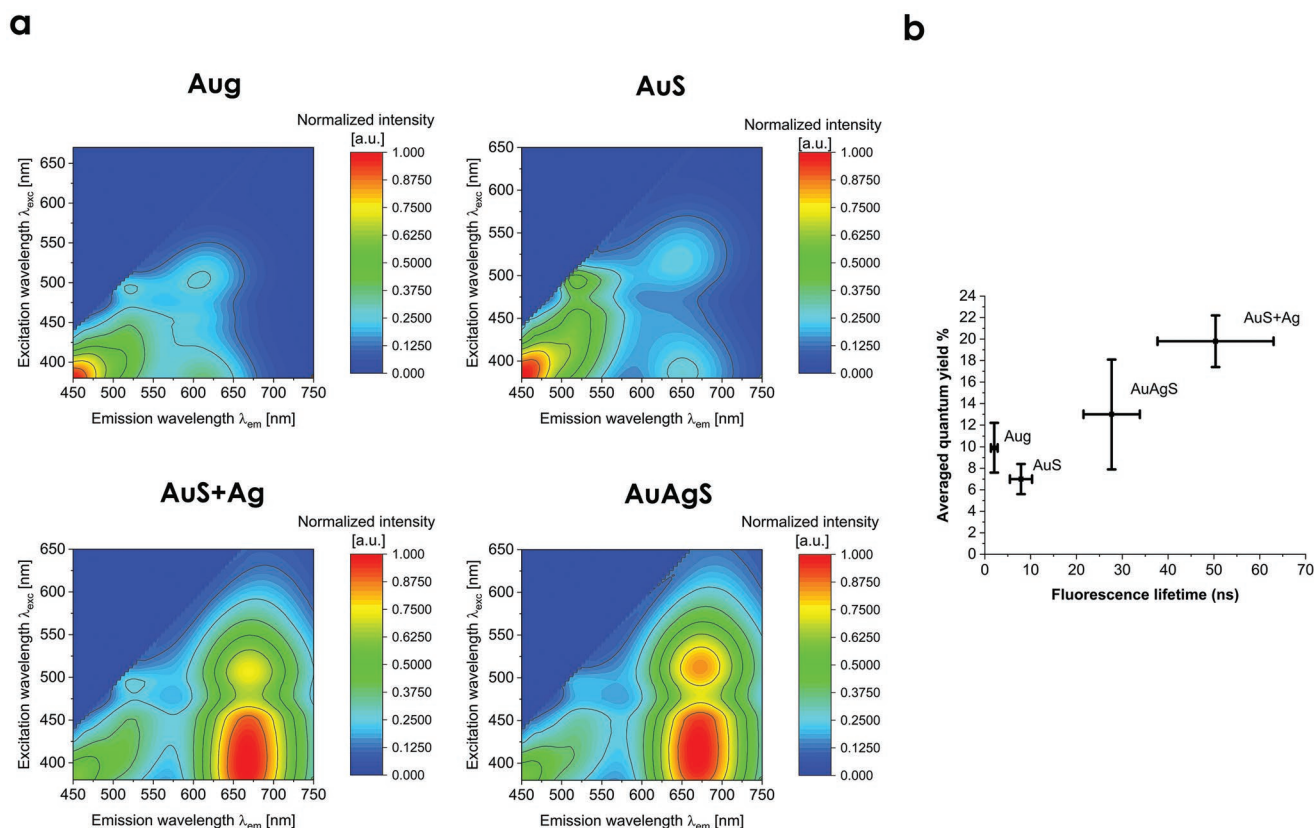


**Figure 4.** Optical properties of different AuNCs; Aug, AuS, AuAgS, and AuS+Ag. a) 3D emission spectra at excitation wavelength range 380–650 nm and the emission was recorded from 450 to 750 nm. b) Averaged lifetime (measured upon excitation at 470 nm) correlation to averaged absolute quantum yield% (measured upon excitation at 400–550 nm with 5 nm steps). The fluorescence around 450–550 nm is due to the gelatin autofluorescence.

nanoclusters. In another strategy, we investigated the addition of Ag ions after completion of the reaction of AuS formulation. Adjustments of the Ag:Au molar ratio, pH, and reaction time have been considered to maximize the fluorescence brightness (Figure S9, Supporting Information). Finally, two Ag-modified formulations; alloy AuNCs (AuAgS) and postsynthesis Ag-modified AuS (AuS+Ag) as in Table S1 (Supporting Information) were selected for further characterization comparing to Aug and AuS. TEM images and measured size distributions are shown in Figures S7 and S10 (Supporting Information) of silver-modified and pure gold nanoclusters, respectively.

3D emission spectra of the four selected formulations are illustrated in Figure 4a. All samples showed broad emission spectra with assigned redshift due to the costabilization with GSH and enhancement of fluorescence upon modification using Ag. Both alloy nanoclusters formation and postsynthesis modification by Ag resulted in enhanced broad red emission bands upon excitation at 380–550 nm. This offers a variety for the nanoclusters application for bioimaging over a wide range of fluorescence imaging settings. Absolute quantum yields (QYs) were measured using integrating sphere setup at different excitation wavelengths (400–550 nm) and were corrected for gelatin's blue fluorescence (Figure S11a, Supporting Information). Modification with Ag resulted in about threefold enhancement in the QY upon excitation at 400 nm in comparison to AuS. The measurements revealed that Ag-modified AuNCs have an excitation-wavelength-dependent QY and

this behavior is more pronounced in AuAgS. They show the maximum QY at 400 nm (24%) that declined to reach the value of AuS ( $\approx 9\%$ ) at 500–550 nm (Figure S11, Supporting Information). Nevertheless, modification by Ag resulted in lower decay rate of fluorescence when excited at 470 nm (Figure S11b, Supporting Information). Interestingly, it turns out that the enhancement of QY after the addition of Ag is correlated to a prolonged fluorescence lifetime (as summarized in Figure 4b).

#### 2.4. Structure–Fluorescence Stability Relationship

Examination of the different AuNCs by XPS provided valuable knowledge about the oxidation state of the metal elements supplying information about the core–shell composition of the nanoclusters. This opens the venue for better understanding of the nanoclusters formation and further correlation to their optical properties and photostability. Starting with Aug, Au 4f doublet can be deconvoluted into 3 distinct components with Au 4f<sub>7/2</sub> at 84.3, 85.3, and 87.6 eV referring to Au (0), Au (I), and Au (III), respectively<sup>[52]</sup> (Figure 5a). So, after 3 h of reaction with gelatin at 60 °C under alkaline conditions, Au (III) has been reduced partially to Au (I) and Au (0) to form AuNCs. However, Au (III)–protein complex has been assigned recently by Dixon and Egusa to also contribute to the fluorescence.<sup>[53]</sup> By virtue to the electron-donating groups in gelatin, Au (I)

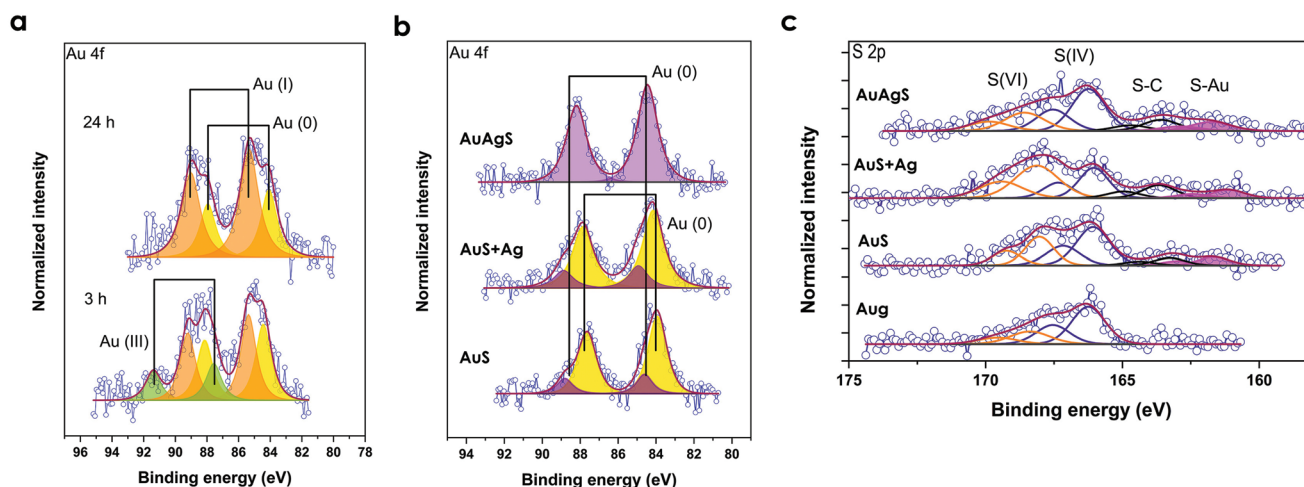


**Figure 5.** XPS spectra. a) Au 4f of AuNCs stabilized by gelatin at different reaction times (3 and 24 h). b) Au 4f of AuNCs stabilized by gelatin and glutathione (AuS, AuS+Ag, and AuAgS from lower to upper panel). Yellow curve: Au (0) at  $84.1 \pm 0.2$  eV, purple curve: Au (0) at  $84.7 \pm 0.2$  eV, orange: Au (I) at  $85.5 \pm 0.2$  eV, green: Au (III). c) S  $2p_{3/2}$  of different AuNCs (AuS, AuS+Ag, and AuAgS from lower to upper panel). Magenta-filled: 161.8 eV (S–Au; S–Ag if present), black: 163.8 eV (S–H), violet: 166.3 eV (oxidized sulfur: S (IV)), orange: 168.6 eV (oxidized sulfur: S (VI)).

as an intermediate reduced state of gold has been produced, with a further reduction to Au (0). The aggregation of Au (0) results in the formation of a metal core with Au (I) on the surface as the nanoclusters' shell as a typical structure described in literature.<sup>[11,27,54]</sup> After 24 h of reaction, all Au (III) has been totally reduced to Au (I) and Au (0) (Figure 5a). On the other hand, coreduction with GSH resulted in complete reduction to Au (0), forming two populations of AuNCs of different core sizes with Au  $4f_{7/2}$  peaks of Au (0) at 83.9 and 84.6 eV (Figure 5b). As previously reported, the higher binding energy of Au (0) indicates an increment in the core size.<sup>[27]</sup> Addition of Ag ions after the formation of AuS resulted in no change in the Au oxidation state with Au (0) peaks at 84.2 and 84.9 eV. Possibly, Ag ions are further reduced by the ligands and incorporated in or replaced some of the Au atoms at the surface of the nanoclusters. Other techniques as X-ray powder diffraction (XRD)<sup>[51]</sup> are required to confirm the atom arrangement within the clusters, however this was not possible with the current formulations due to the very minute amount of Ag and Au compared to the gelatin matrix. Similarly, complete reduction of Au has been observed with the formation of alloy NCs (AuAgS), but interestingly with homogenous-sized population of AuNCs (Au  $4f_{7/2}$  showed one peak at 84.5 eV) (Figure 5b). However, we cannot provide any evidence of Ag reduction especially with the difficulty to distinguish between Ag  $3d_{5/2}$  corresponding to Ag (0) and Ag (I) without Auger line analysis, which was hindered by the very low concentration of Ag (Figure S12, Supporting Information) near the detection limit. Coreduction with GSH showed S 2p doublet with S  $2p_{3/2}$  at 161.8 eV (S–Au; S–Ag if present),<sup>[55]</sup> 163.8 eV (S–H), 166.2 eV (oxidized sulfur: S (IV)) and 168.6 eV (oxidized sulfur: S (VI))<sup>[56]</sup> (Figure 5c) with very weak concentrations of 0.02, 0.03, 0.09, and 0.05 at% in AuAgS, respectively. A possible Au–S bond may be formed; however data must be taken with caution due to the very low concentration of these elements, as the bulk of the sample constitutes out of gelatin, and the detection limit of the method. But on the other hand, the concentrations of Au and Ag were found in

the same range with values of 0.02 and 0.01 at%, respectively, which supports the assumption of formed Au–S and eventually Ag–S bonds.

AuNC structure together with the ligand plays the main role in controlling their optical properties due to electron transfer between the ligand and the metal surface and within the metal core. On the other hand, ligands as capping agents control the stability of the AuNC fluorescence in response to the different environmental conditions. Testing the robustness of AuNC fluorescence over a pH range (1.5–7) in comparison to the original synthesis environment, showed different degrees of stability arranged in the following order  $\text{AuS} < \text{AuS+Ag} < \text{AuAgS}$  (Figure 6a). However, all AuNCs showed considerable fluorescence stability at physiological pH; modifications with GSH and Ag have widened the pH stability range down to acidic conditions. Possessing the capability to manipulate the pH response of AuNCs provides the opportunity for various applications. For instance, the pH responsiveness showed by AuS could be utilized as a bioprobe to monitor pH changes in cancer cells.<sup>[57]</sup>

To investigate the contribution of gelatin and GSH in stabilizing AuNCs, a trypsination experiment has been performed. Trypsin works specifically by hydrolyzing the peptide bonds on the carboxylic terminal of lysines and arginines. According to the trypsin concentration and the amino acid sequence of the protein, the maximum degree of hydrolysis varies.<sup>[58]</sup> In case of AuS, gelatin is the main reducing and capping agent for AuNCs. Gelatin fragmentation by trypsin resulted in drop of the fluorescence that was trypsin-concentration-dependent, as shown in Figure 6b. When the polypeptide loses its structure integrity that was responsible for holding the gold atoms and ions together, they dissociate and the fluorescence diminishes as observed at trypsin activity of  $3.2 \times 10^3$  U  $\text{mg}^{-1}$  of gelatin. Interestingly, AuS fluorescence showed much higher stability to trypsin digestion. It can be envisaged that even after gelatin digestion, the AuNC structure is still preserved by binding to the thiolate groups of GSH and fractions of degraded gelatin.

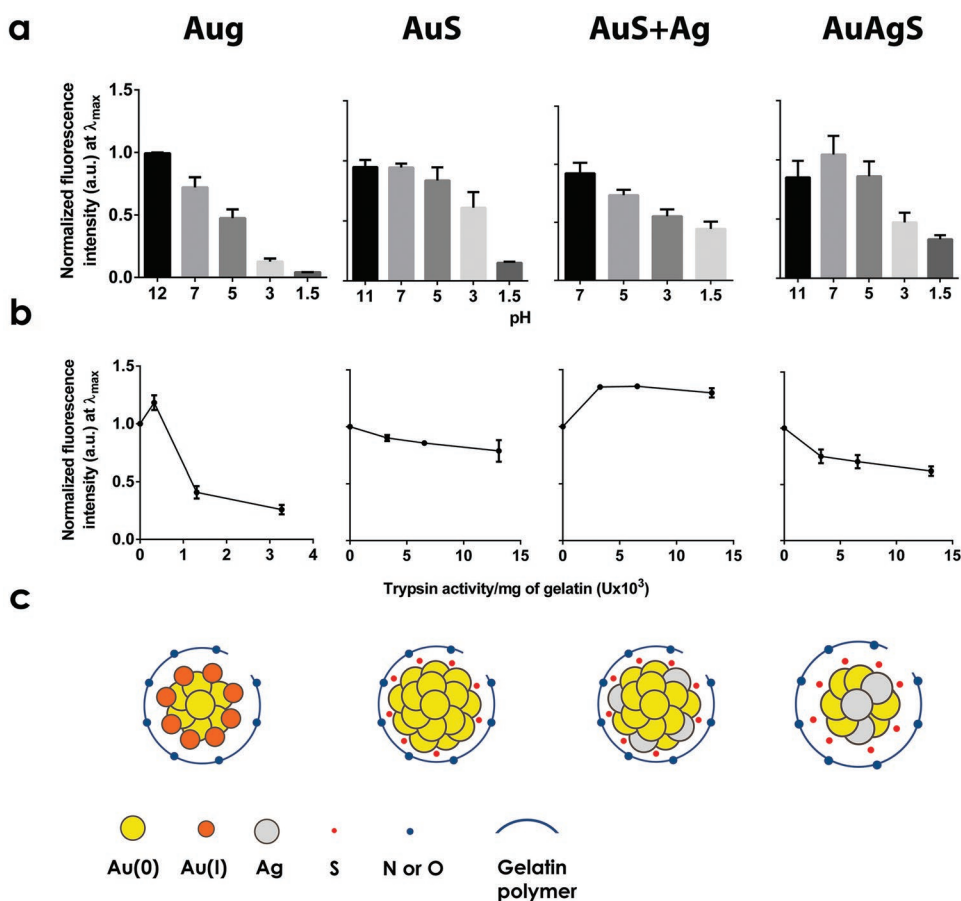


**Figure 6.** Fluorescence stability of different AuNC against a) pH changes upon altering the pH from that of synthesis to lower pH values (1.5–7), b) gelatin digestion using different concentrations of trypsin at pH 7.4, 37 °C for 15 h. Fluorescence intensity was recorded at  $\lambda_{max}$  for the different AuNCs (640 nm for Aug, 690 nm for AuS, and 700 nm for both AuS+Ag and AuAgS). This shows the effect of GSH and Ag ion addition on enhancing the AuNCs fluorescence stability against pH changes and trypsinization. c) Simplified proposed models for AuNC structure based on XPS data. Aug: showed a typical core–shell structure of Au (0) and Au (I), respectively. For all others, GSH-modified AuNCs, Au (0) was the only oxidation state with Au–S bonding. The AuNCs have different core sizes (the biggest; AuS and the smallest AuAgS) referring to the Au (0) binding energy of 83.9 and 84.5 eV, respectively.

This provides valuable information about the role of both gelatin and GSH in AuNC protection. Whereas AuAgS showed intermediate stability to gelatin, AuS+Ag showed ultimate stability (Figure 6b). The latter even showed a slight increase in fluorescence, probably due to trypsin adsorption to the AuNCs.<sup>[59–61]</sup> This formulation will be interesting for long-term imaging of AuNCs in tissues due to their stability regardless of the integrity of gelatin as capping agent. On the other hand, AuAgS would be beneficial for mechanistic studies, especially when formulated as GNPs. Their bright fluorescence alongside with their intermediate sensitivity to polymer degradation will be a beneficial option to smartly track the NPs and follow their fate in tissues. In conclusion, NCs can offer stimuli-responsive fluorescence, i.e., are smart probes (different response to pH, enzymatic degradation, etc.), which can be manipulated by controlling the NC and ligand compositions. This is an advantage of such imaging probes over standard dyes, where different stimuli responsiveness need careful selection of more than one dye to fulfill the same functions.

From the knowledge gained throughout the characterization of the different AuNCs' optical properties and XPS

studies introduced in this research work, accompanied with knowledge from literature about the general structure of gold nanoclusters,<sup>[11,13,54]</sup> simplified models for the nanoclusters have been proposed, as shown in Figure 6c. Aug, where nanoclusters are produced only using gelatin, is considered the parent formulation that is further modified to other formulations with different properties. These clusters showed a typical core–shell structure composed of Au (0) and Au (I) protected by gelatin as the only ligand. Further, addition of GSH resulted in complete reduction of Au (III) to Au (0) and nanoclusters formation of two different sizes. Additionally, GSH stabilization provided higher protection of the nanocluster fluorescence toward pH change and enzymatic degradation. Addition of Ag ions after or during the synthesis of AuS resulted in enhancement of the fluorescence intensity, QY, lifetime, and stability. Addition of Ag after the synthesis of AuS (AuS+Ag) led to no changes in the oxidation state of Au and some incorporation of Ag in the nanocluster surface. On the other hand, addition of Ag ions during the synthesis process of AuS seems to lead to the formation of smaller alloy nanoclusters (AuAgS) but of homogenous size.

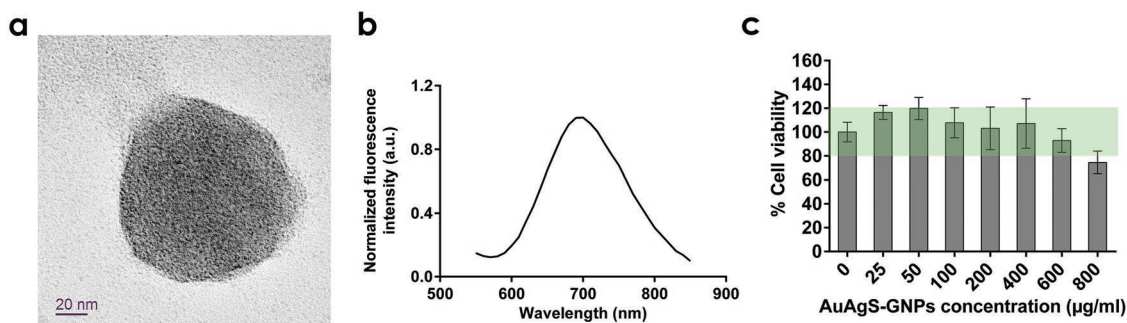


**Figure 7.** a) TEM image of AuAgS-GNPs with accelerating voltage 100 kV. b) Emission spectrum of the nanoparticles by excitation at 368 nm. c) Cytotoxicity testing of AuAgS-GNPs against human keratinocytes (HaCat cells) using different concentrations (25–800  $\mu\text{g mL}^{-1}$ ) by MTT assay. Green-shaded box indicates the range where no toxicity is concluded.

## 2.5. Formation of Protein Nanoparticles Using AuNC-Modified Gelatin

Such NPs were prepared by two-step desolvation method using AuNC-modified gelatin. Desolvation is the dehydration of gelatin by addition of an antisolvent, which results in coiling of the polypeptide chains. The first desolvation step was to separate the gelatin fractions of high molecular weight (HMW). Discarding the low molecular weight fractions of gelatin will enhance the homogeneity of the NP size and prevent irreversible aggregation.<sup>[62]</sup> The redissolved HMW gelatin was desolvated again to form NPs that were further cross-linked to preserve their conformation in aqueous environment. Different parameters have been optimized such as the antisolvent, the pH of gelatin solution, and the cross-linking agent.

NP formation is a complex phenomenon controlled by the polymer–antisolvent–solvent system. The diffusion and the affinity of the antisolvent to solvent and the polymer–solvent interactions influence the particle size.<sup>[63]</sup> Among different organic solvents (acetone, acetonitrile, isopropanol, ethanol), only methanol was suitable for AuNC-modified GNP formation. At the first desolvation step, pH of gelatin solution was adjusted to 7 to balance between preserving the fluorescence of AuAgS and reducing the charge of gelatin to induce precipitation, while in the second desolvation, the pH was tuned to 8 to prevent NP aggregation. For cross-linking, glutaraldehyde, which is a common cross-linker for GNPs, resulted in complete loss of the Aug-modified GNP fluorescence, in agreement to a previous report by Khandelia et al.<sup>[64]</sup> This can be attributed to the cross-linking mechanism of glutaraldehyde which is a non-zero length cross-linker that connects the alpha-amino groups of lysine residues.<sup>[65]</sup> Consequently, another cross-linker has been applied to preserve the fluorescence. This was a combination of *N*-(3-dimethylaminopropyl)-*N*'-ethylcarbodiimide hydrochloride (EDC) and *N*-hydroxysuccinimide (NHS); which is a zero-length cross-linking agent that couples carboxylic to primary amine groups.<sup>[66]</sup>

Nanoparticles of narrow particle size distribution have been produced using Aug, AuS (Figure S13, Supporting Information), and AuAgS-modified gelatin (Figure 7a). TEM showed the NPs nicely spherical in shape and non-aggregated and it, amazingly, revealed the internal distribution of the AuNCs. Among them, AuAgS-GNPs were of interest for further studies with Z-average size =  $218.8 \pm 1.7$  nm and a size distribution displayed

by the polydispersity index (PDI) of  $0.073 \pm 0.016$ . They showed high colloidal stability and further freeze drying with trehalose had no effect on the particle size following redispersion. The NP formation preserved the fluorescence emission spectrum of AuAgS (Figure 7b). Absolute QY was measured ( $\lambda_{\text{max}} = 400\text{--}550$  nm) and corrected for the NP scattering using similar plain GNPs as a reference. They showed averaged QY =  $14.8 \pm 0.8\%$  which was excitation-wavelength-independent, in contrast to the free nanoclusters. However, the formation of NPs have not changed the fluorescence lifetime behavior, as AuAgS-GNPs showed higher fluorescence lifetime in comparison to Aug and AuS-GNPs (Figure S15, Supporting Information).

The cytotoxicity of AuAgS-GNPs has been tested against human keratinocytes (HaCat cell line) using 3-(4,5-Dimethylthiazol-2-yl)-2,5-diphenyltetrazolium bromide (MTT) assay, which assesses the cell metabolic activity, after 24 h of incubation. The NPs showed no cytotoxicity ( $\approx 100\%$  viability) at concentrations as high as  $600 \mu\text{g mL}^{-1}$  (Figure 7c). This can be attributed to the biocompatibility of the materials used in the preparation including the nontoxic cross-linking agent (EDC). Concerns have been considered about the reported toxicity of silver ions. Nevertheless, the formulation was biocompatible, due to the very minute amount used, and the possible complete reduction of Ag ions during the nanoclusters preparation. Finally, the produced fluorescent GNPs are safe biomaterials that pave the way for various biological applications including drug delivery.

## 2.6. Tissue Bioimaging Based on Linear Unmixing

Imaging and tracking of NPs in tissue using confocal laser scanning microscopy (CLSM) is a complex, even though beneficial process, which provides deeper knowledge about nanopharmaceutical efficiency and fate. In this regard, we have selected human skin to test the ability of our developed AuAgS-labeled GNPs to be imaged with tissue. Skin is known as a challenging tissue for imaging due to its density and autofluorescence that limit the process of suitable dye selection. Additionally, this imaging probe opens the avenue for better understanding of NP behavior in skin. This will be helpful for therapeutic purposes through transdermal drug delivery which gains a lot of attention recently to take over the invasive methods. On the other hand, occupational nanomaterial skin exposure can be hazardous for



human health, especially over a long term. Overall, the developed fluorescent GNPs can be further applied to different biological applications that can even extend from skin to other tissues.

There are many endogenous autofluorescent substances in skin that may interfere with the analysis of different fluorophores. This renders the choice of a suitable fluorophore, with a distinct fluorescence from that of skin, not an easy option, especially due to the broad emission spectrum of skin. Even with suitable dyes, offsetting the skin's fluorescence was the solution used by different research groups for imaging of NPs in skin.<sup>[67–70]</sup> However, the ability to image NPs together with skin structure will give visual evidence about the NP penetration within the tissue. In this regard, others resort to either dual-channel imaging followed by subsequent images overlapping,<sup>[71]</sup> or staining of skin prior to NP examination.<sup>[72]</sup> AuAgS–GNPs showed well-detected fluorescence in the red region of the spectrum (Figure 8a). This can be considered as the optimum properties of a fluorophore for imaging with skin. However, imaging of both NPs and skin simultaneously will be a more descriptive and time-saving method of analysis.

Linear unmixing is a technique that is used for separation of the signals of fluorophores of overlapping spectra. An algorithm is applied to analyze each pixel and segregate the mixed fluorescence signals arising from multiple fluorophores into individual components accrediting to spectral reference fingerprints.<sup>[73]</sup> AuAgS–GNPs showed a distinct fluorescence signal from that of skin (Figure 8a). Instead of canceling the skin fluorescence, linear unmixing has been utilized to separate NPs from skin signal. To test the accuracy of the method, NPs have been added to the skin surface and imaged directly. Figure 8b shows  $\approx 200 \mu\text{m}$  depth profiling (z-stack steps of  $5 \mu\text{m}$ ) of the NPs and skin, while 3D-constructed images are shown in Figure 8c. The images showed the NPs filling the furrows of the skin between the keratinocyte isles in a similar pattern to results shown earlier by Stracke et al.<sup>[74]</sup> This indicates the applicability of the method for accurately separating the signals, so penetration studies within the tissue can be further analyzed.

Microneedles have been widely used as a minimally invasive mechanical penetration method to deliver biotherapeutics through skin.<sup>[75]</sup> The nanocarriers labeled with NPs were loaded in dissolving microneedles composed of polyvinyl alcohol (PVA)/sucrose. After microneedle insertion in skin, linear unmixing revealed the NP distribution within the skin tissue with a depth profile of  $760 \mu\text{m}$  (Figure 8d). So, spectral imaging with linear unmixing offers a time-saving, noninvasive, and depth-revealing technique for simultaneous examination of the NPs and skin, which helps to avoid the artifacts produced during skin sectioning and staining. Finally, the developed AuNC-modified GNPs showed to be an effective fluorescent probe for bioimaging with biological tissue such as skin. The developed nanoparticulate system with assistance of minimally invasive techniques as microneedle application, will be further investigated for delivering antigen through skin for transcutaneous vaccination with the ability of simultaneous bioimaging and particle tracking.

### 3. Conclusion

We proved the effectiveness of gelatin to produce fluorescent AuNCs, introducing different methods for tuning the emission

wavelength alongside with the fluorescence intensity. Gold ions reduction-assisted by GSH, in one-pot synthesis, induced 50 nm redshift in the nanoclusters emission alongside with stabilization against pH changes and enzymatic degradation. Modification by Ag ions either by doping during or post the nanoclusters formation resulted in enhancement of the QY and fluorescence lifetime. Finally as a result, four different AuNCs have been produced, showing variant stability in response to pH and enzymatic degradation, so they can be acclaimed for various biological applications. The optical properties–structure relationship has been established with the aid of XPS analysis. Model structures for the different formulated AuNCs have been constructed, summarizing the effect of different modifications. On the other hand, optimization of the synthesis process resulted in preserving the gelatin structure integrity, to be further efficiently used for the preparation of GNPs. The NPs of size 218 nm showed distinct inner distribution of the AuNCs when examined by TEM. They preserved the fluorescence properties of the nanoclusters, thanks to the careful selection of the cross-linking agent (EDC/NHS). They showed biocompatibility toward human keratinocyte cell line up to  $600 \mu\text{g mL}^{-1}$ , which acclaims them for further applications in drug delivery. They have been imaged simultaneously with skin fluorescence using noninvasive time-saving method by combining CLSM and linear unmixing, achieving a depth profile of  $760 \mu\text{m}$ . Finally, our study can be considered as a platform for putting insights into the design, optimization, and better understanding of the AuNC formation and properties. The development of AuNC-modified GNPs represents a very promising approach for imaging in a challenging tissue as skin that can extend to various theranostic and pharmaceutical applications, preferably antigen delivery for transcutaneous vaccination.

### 4. Experimental Section

**Materials:** Hydrogen tetrachloroaurate (III) trihydrate ( $\text{HAuCl}_4 \cdot 3\text{H}_2\text{O}$ ), gelatin type B (from bovine skin, gel strength  $\approx 75 \text{ g Bloom}$ ), silver nitrate, EDC, NHS, D-(+)-trehalose dihydrate, PVA (Mowiol 4-88, Mw  $\approx 31\,000$ ), sucrose, methanol, dimethyl sulfoxide (DMSO) were all purchased from Sigma-Aldrich, Steinheim Germany. Ninhydrin (2,2-dihydroxyindane-1,3-dione) was purchased from Merck, Darmstadt, Germany. Trypsin from bovine pancreas (activity:  $3273.4 \text{ U mg}^{-1}$ ) was obtained from PanReac Applichem, Darmstadt, Germany. All chemicals were utilized without further purification. Milli-Q ultrapure water was used for all experiments.

**Synthesis of Gelatin-Stabilized AuNCs:** Gold nanoclusters stabilized by gelatin were prepared by adding  $\text{HAuCl}_4$  to gelatin solution followed by adjusting the pH using 1 N sodium hydroxide. The reaction was carried out for 24 h under vigorous mixing in a thermomixer (MHR, Hettich Benelux, Geldermalsen, The Netherlands) at  $60 \text{ }^\circ\text{C}$ . Different  $\text{HAuCl}_4$  concentrations ( $1 \times 10^{-3}$ – $20 \times 10^{-3} \text{ M}$ ) and different pH values (7–12) were tested for AuNC formation evaluated by fluorescence evolution. The optimized nanoclusters (AuG) were utilized for further investigations.

**Synthesis of Gelatin-Stabilized AuNCs Modified by Glutathione:** In one-pot reaction, GSH with different concentrations ( $5 \times 10^{-3}$ – $25 \times 10^{-3} \text{ M}$ ) was added to 4% w/v gelatin, followed by addition of  $10 \times 10^{-3} \text{ M}$   $\text{HAuCl}_4$ . All other settings were adjusted as shown before and the reaction proceeded for 24 h. The optimized formulation (AuS) was applied for further modifications as will be shown later.

**Gelatin Structure Integrity:** Selected formulations showing the highest fluorescence were repeated following the previously mentioned procedure while varying the reaction times (1–24 h). The fluorescence at the maximum wavelength was plotted against time and further

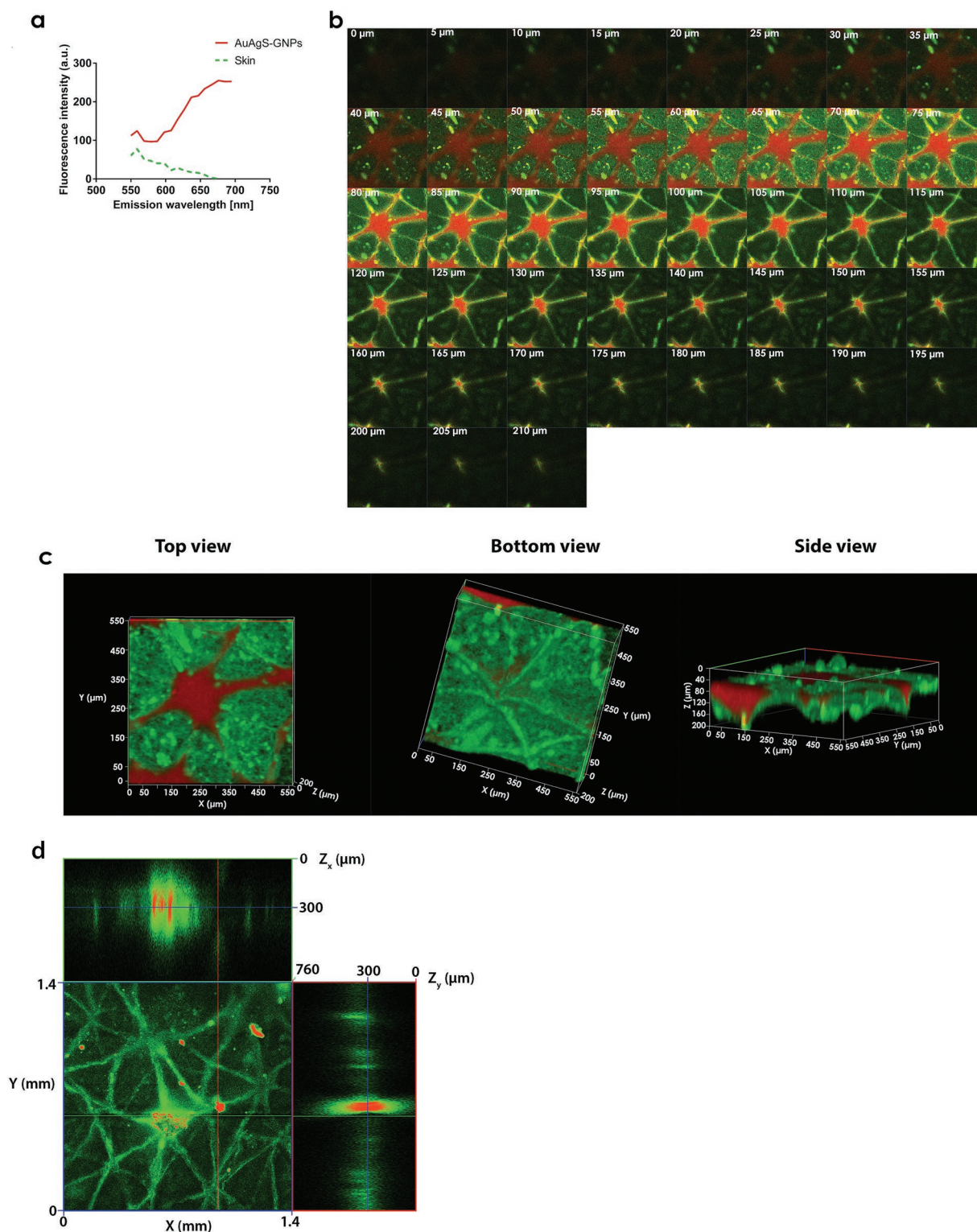


**Figure 8.** a) Emission spectra of skin and AuAgS-GNPs recorded by confocal microscopy at  $\lambda_{\text{ex}}$  405 nm. b,c) 3D confocal imaging of NPs applied to the skin surface. (b) z-stacks starting from skin surface to 210  $\mu\text{m}$  depth in tissue with 5  $\mu\text{m}$  steps. This shows the NPs (red) filling the furrows between the keratinocyte isles (green). The fluorescence channels were separated from the crude fluorescence using linear unmixing algorithm with reference to the fluorescence spectra of skin and NPs. (c) 3D images constructed from the z-stacks showing upper, bottom, and side view (from left to right) of the scanned area. d) 3D confocal imaging of NP-loaded microneedles applied into skin, constructed from z-stacks recorded over 760  $\mu\text{m}$  depth with 10  $\mu\text{m}$  steps, showing the NPs (red) penetration depth ( $Z_x$  and  $Z_y$ ) into skin tissue (green). The XY-plane shows a horizontal cut at 300  $\mu\text{m}$  depth displaying the nanoparticle distribution.

the samples were examined for gel formation after cooling to 4 °C. The free amine groups in gelatin were quantified by ninhydrin test over different time intervals of interaction with gold. Briefly, pH of AuNC-modified gelatin was adjusted to 7 by 1 N HCl and mixed vigorously (1000 rpm) with 3% ninhydrin solution in 90% DMSO at 80 °C for 5 min. Then, the mixture was cooled down to room temperature for 30 min and absorbance was measured at 575 nm. Calibration curve was constructed using glycine as a standard<sup>[76]</sup> following the same procedure. FT-IR and MALDI-TOF MS were performed. Freeze-dried samples of selected AuNC-modified gelatin were scanned for their FT-IR spectrum between 4000 and 400 cm<sup>-1</sup> (Spectrum 400, FT-IR/FT-NIR Spectrometer, PerkinElmer, Rodgau, Germany). For MALDI-TOF MS, samples were analyzed in positive mode with a matrix of sinapinic acid using Applied Biosystems 4800 MALDI TOF/TOF analyzer (Applied Biosystems, Warrington, Cheshire, UK).

**Synthesis of Ag-Modified AuNCs Stabilized by Gelatin and Glutathione:** The GSH-modified gelatin-stabilized AuNCs synthesized after optimized conditions (AuS) were further modified using silver ions following two different protocols. I) To form alloy metal NCs, AgNO<sub>3</sub> was added during the formation of the nanoclusters. Effect of different Ag/Au ratios, reaction times and pH was tested. II) To modify the surface of AuNCs, AgNO<sub>3</sub> was added after the synthesis of AuNCs. For screening, fluorescence spectra were recorded for all tested formulations (550–850 nm) upon excitation at 368 nm using Microplate reader (Infinite M200, Tecan Group Ltd., Männedorf, Switzerland).

**Characterization of Selected AuNC Formulations:** 3D-fluorescence spectra, time-correlated single photon counting, alongside with the fluorescence quantum yield measurement were performed. Further details for the setup can be found in the Supporting Information. Fluorescence imaging was carried out by confocal microscope (LSM 710, Zeiss, Jena, Germany) using excitation laser of 405 nm and emission was detected between 600 and 740 nm. TEM was performed using a JEOL Model JEM 2010 microscope (JEOL GmbH, Freising, Germany). Robustness of AuNC fluorescence against changes in environmental conditions (pH and enzymatic activity) was tested. The emission at the maximum wavelength was recorded upon excitation at 368 nm for the as prepared AuNCs and after pH change. On the other hand, AuNCs in PBS (pH 7.4, 5 mg mL<sup>-1</sup>) were mixed with different concentrations of trypsin solutions at 500 rpm and 37 °C for 15 h. Fluorescence was recorded before and after reaction with trypsin.

**XPS Analysis:** Samples' pH was adjusted to 7, freeze-dried, and then analyzed using a KAlpha+ spectrometer (ThermoFisher Scientific, East Grinstead, UK) equipped with a microfocussed, monochromated Al K $\alpha$  X-ray source (400  $\mu$ m spot size). The charge compensation system was applied using electrons of 8 eV energy and low-energy argon ions to prevent any localized charge buildup. The electrons' kinetic energy was measured by a 180° hemispherical energy analyzer in the constant analyzer energy mode at 50 eV pass energy. Data acquisition and processing using the Thermo Avantage software was described elsewhere.<sup>[77]</sup> The Scofield sensitivity factors were applied for quantification.<sup>[78]</sup> All spectra were referenced to the C 1s peak at 285.0 eV binding energy (C–C, C–H).

**Preparation of AuNC-Modified GNPs:** They were fabricated using two-step desolvation method and cross-linking. For the first precipitation, methanol was added to the AuNC-modified gelatin and shaken to precipitate the high molecular weight fractions and the turbid supernatant was discarded. The gel-like mass of gelatin was freeze-dried, weighed, and dissolved in water at 50 °C, giving rise to 2% w/v solution. The pH of gelatin solution was adjusted to 8 using 1 N NaOH and methanol was added dropwise while stirring until the first turbidity was observed, indicating the formation of NPs. They were further cross-linked using a mixture of EDC/NHS that was added dropwise. The NP dispersion was kept under stirring at 600 rpm for 18 h. They were purified by centrifugation (Thermo Fisher Scientific, Osterode am Harz, Germany) at 20 000  $\times$  g for 1 h at 20 °C followed by washing that was repeated 3 times. Following, the NP dispersion was freeze-dried using 3% w/v trehalose as a cryoprotectant to be further used for other experiments.

**Cell Culture:** Human keratinocytes cell line (HaCaT) was cultured in Dulbecco's modified Eagle's medium (Gibco, Thermo Fischer Scientific, Paisley, UK) supplemented with 10% v/v fetal calf serum and 100 U mL<sup>-1</sup> penicillin–streptomycin. The cells were incubated at 37 °C under 5% CO<sub>2</sub>. Cytotoxicity of the selected Ag–Au alloy NC (AuAgS)-modified GNPs was tested using MTT assay for cell viability. Further details can be found in the Supporting Information.

**Bioimaging of GNPs with Skin Tissue:** Excised human skin was obtained from abdominal plastic surgeries after the approval of the Research Ethic Committee of Saarland, Germany (Ärzttekammer des Saarlandes, Dec. 2008) and permission of the volunteers. Further details about skin preparation and the examination setup can be found in the Supporting Information. First, untreated human skin samples and AuAgS-modified GNPs were separately scanned for their emission spectrum in the range 600–740 nm by confocal microscopy using lambda mode upon excitation at 405 nm. The treated skin samples were tested applying the same parameters. Two groups of skin samples were treated with AuAgS-modified GNPs; a) by addition of NPs to skin surface and b) by insertion of AuAgS-modified GNP-loaded microneedles into skin. Using the linear unmixing algorithm available in the Zen Black software, the fluorescence signals of the NPs were separated from that of skin. For depth profiling, objectives (LCI Plan-Neofluar 25 $\times$ /0.8 Imm Korr DIC M27 and EC Plan-Neofluar 10 $\times$ /0.3 M27) have been used and z-stacks were recorded with 5 and 10  $\mu$ m steps for the surface and microneedle applications, respectively, and 3D images were constructed.

## Supporting Information

Supporting Information is available from the Wiley Online Library or from the author.

## Acknowledgements

The authors acknowledge the Egyptian Ministry of Higher Education, Culture Affairs and Missions Sector (MOHE-CASM) for funding. The purchase of the XPS KAlpha+ instrument was financially supported by the Federal Ministry of Economics and Technology on the basis of a decision by the German Bundestag. The authors thank Aljoscha Könnike and Dr. Marcus Koch for helping with TEM imaging and Dr. Robert Haberkorn for the XRD experiments.

## Conflict of Interest

The authors declare no conflict of interest.

## Keywords

drug delivery, fluorescent enhancement, nanotechnology, protein-stabilized gold nanoclusters, theranostics

Received: July 26, 2019  
Revised: November 9, 2019  
Published online:

- [1] F. Xia, W. Hou, C. Zhang, X. Zhi, J. Cheng, J. M. de la Fuente, J. Song, D. Cui, *Acta Biomater.* **2018**, *68*, 308.
- [2] Y. Chen, D. M. Montana, H. Wei, J. M. Cordero, M. Schneider, X. Le Guével, O. Chen, O. T. Bruns, M. G. Bawendi, *Nano Lett.* **2017**, *17*, 6330.
- [3] Y. Wang, L. Hu, L. Li, J.-J. Zhu, *J. Anal. Test.* **2017**, *1*, 13.
- [4] Y. Sun, J. Wu, C. Wang, Y. Zhao, Q. Lin, *New J. Chem.* **2017**, *41*, 5412.

- [5] Y. Pan, Q. Li, Q. Zhou, W. Zhang, P. Yue, C. Xu, X. Qin, H. Yu, M. Zhu, *Talanta* **2018**, *188*, 259.
- [6] A. Biswas, S. Banerjee, E. V. Gart, A. T. Nagaraja, M. J. McShane, *ACS Omega* **2017**, *2*, 2499.
- [7] J. R. Lakkakula, D. Divakaran, M. Thakur, M. K. Kumawat, R. Srivastava, *Sens. Actuators, B* **2018**, *262*, 270.
- [8] K. Zheng, M. I. Setyawati, D. T. Leong, J. Xie, *ACS Nano* **2017**, *11*, 6904.
- [9] A. Yahia-Ammar, D. Sierra, F. Mérola, N. Hildebrandt, X. Le Guével, *ACS Nano* **2016**, *10*, 2591.
- [10] P. Zhang, *J. Phys. Chem. C* **2014**, *118*, 25291.
- [11] D. M. Chevrier, R. Yang, A. Chatt, P. Zhang, *Nanotechnol. Rev.* **2015**, *4*, 193.
- [12] S. Palmal, R. Jana Nikhil, *Wiley Interdiscip. Rev.: Nanomed. Nanobiotechnol.* **2014**, *6*, 102.
- [13] D. Li, Z. Chen, X. Mei, *Adv. Colloid Interface Sci.* **2017**, *250*, 25.
- [14] A. Cantelli, G. Battistelli, G. Guidetti, J. Manzi, M. Di Giosia, M. Montalti, *Dyes Pigm.* **2016**, *135*, 64.
- [15] D. Bain, S. Maity, B. Paramanik, A. Patra, *ACS Sustainable Chem. Eng.* **2018**, *6*, 2334.
- [16] Z. Wu, R. Jin, *Nano Lett.* **2010**, *10*, 2568.
- [17] G. Pramanik, J. Humpolickova, J. Valenta, P. Kundu, S. Bals, P. Bour, M. Dracinsky, P. Cigler, *Nanoscale* **2018**, *10*, 3792.
- [18] M. G. Warner, S. M. Reed, J. E. Hutchison, *Chem. Mater.* **2000**, *12*, 3316.
- [19] Y. Xu, J. Sherwood, Y. Qin, D. Crowley, M. Bonizzoni, Y. Bao, *Nanoscale* **2014**, *6*, 1515.
- [20] Y. Bai, Y. Zhou, H. Liu, L. Fang, J. Liang, S. Xiao, *ACS Appl. Nano Mater.* **2018**, *1*, 969.
- [21] L. Kong, X. Chu, X. Ling, G. Ma, Y. Yao, Y. Meng, W. Liu, *Microchim. Acta* **2016**, *183*, 2185.
- [22] L. Polavarapu, M. Manna, Q.-H. Xu, *Nanoscale* **2011**, *3*, 429.
- [23] B.-Y. Wu, C.-W. Wang, P.-C. Chen, H.-T. Chang, *Sens. Actuators, B* **2017**, *238*, 1258.
- [24] C. Zhang, Z. Zhou, Q. Qian, G. Gao, C. Li, L. Feng, Q. Wang, D. Cui, *J. Mater. Chem. B* **2013**, *1*, 5045.
- [25] L.-Y. Chen, C.-W. Wang, Z. Yuan, H.-T. Chang, *Anal. Chem.* **2015**, *87*, 216.
- [26] K.-T. Chuang, Y.-W. Lin, *J. Phys. Chem. C* **2017**, *121*, 26997.
- [27] X. Le Guével, B. Hötzer, G. Jung, K. Hollemeyer, V. Trouillet, M. Schneider, *J. Phys. Chem. C* **2011**, *115*, 10955.
- [28] B. A. Russell, B. Jachimska, I. Kralka, P. A. Mulheran, Y. Chen, *J. Mater. Chem. B* **2016**, *4*, 6876.
- [29] S. Yang, Z. Jiang, Z. Chen, L. Tong, J. Lu, J. Wang, *Microchim. Acta* **2015**, *182*, 1911.
- [30] Q. Yue, L. Sun, T. Shen, X. Gu, S. Zhang, J. Liu, *J. Fluoresc.* **2013**, *23*, 1313.
- [31] T. Zhao, Z. Q. Xuan, A. Wan, R. Gui, *Mater. Technol.* **2016**, *31*, 342.
- [32] C.-L. Liu, H.-T. Wu, Y.-H. Hsiao, C.-W. Lai, C.-W. Shih, Y.-K. Peng, K.-C. Tang, H.-W. Chang, Y.-C. Chien, J.-K. Hsiao, J.-T. Cheng, P.-T. Chou, *Angew. Chem., Int. Ed.* **2011**, *50*, 7056.
- [33] P.-F. Chen, C.-L. Liu, W.-K. Lin, K.-C. Chen, P.-T. Chou, S.-W. Chu, *Biomed. Opt. Express* **2015**, *6*, 3066.
- [34] H. Kawasaki, K. Yoshimura, K. Hamaguchi, R. Arakawa, *Anal. Sci.* **2011**, *27*, 591.
- [35] J.-M. Liu, J.-T. Chen, X.-P. Yan, *Anal. Chem.* **2013**, *85*, 3238.
- [36] D. Lu, L. Liu, F. Li, S. Shuang, Y. Li, M. M. F. Choi, C. Dong, *Spectrochim. Acta, Part A* **2014**, *121*, 77.
- [37] B. A. Russell, B. Jachimska, P. Komorek, P. A. Mulheran, Y. Chen, *Phys. Chem. Chem. Phys.* **2017**, *19*, 7228.
- [38] Y. Xu, S. Palchoudhury, Y. Qin, T. Macher, Y. Bao, *Langmuir* **2012**, *28*, 8767.
- [39] I. Nandi, S. Chall, S. Chowdhury, T. Mitra, S. S. Roy, K. Chattopadhyay, *ACS Omega* **2018**, *3*, 7703.
- [40] N. Sahoo, R. K. Sahoo, N. Biswas, A. Guha, K. Kuotsu, *Int. J. Biol. Macromol.* **2015**, *81*, 317.
- [41] A. Samanta, Y. Zhou, S. Zou, H. Yan, Y. Liu, *Nano Lett.* **2014**, *14*, 5052.
- [42] Y. Liu, X. Liu, X. Wang, *Nanoscale Res. Lett.* **2010**, *6*, 22.
- [43] N. Wangoo, K. K. Bhasin, S. K. Mehta, C. R. Suri, *J. Colloid Interface Sci.* **2008**, *323*, 247.
- [44] S. Van Vlierberghe, G. J. Graulus, S. Keshari Samal, I. Van Nieuwenhove, P. Dubruel, in *Biomedical Foams for Tissue Engineering Applications* (Ed: P. A. Netti), Woodhead Publishing, Sawston, Cambridge, UK **2014**, pp. 335–390.
- [45] B. H. Lee, N. Lum, L. Y. Seow, P. Q. Lim, L. P. Tan, *Materials* **2016**, *9*, 797.
- [46] S. Suarasan, M. Focsan, O. Soritau, D. Maniu, S. Astilean, *Colloids Surf., B* **2015**, *132*, 122.
- [47] K. M. Harkness, D. E. Cliffl, J. A. McLean, *Analyst* **2010**, *135*, 868.
- [48] A. Barth, *Biochim. Biophys. Acta, Bioenerg.* **2007**, *1767*, 1073.
- [49] X. Le Guével, V. Trouillet, C. Spies, K. Li, T. Laaksonen, D. Auerbach, G. Jung, M. Schneider, *Nanoscale* **2012**, *4*, 7624.
- [50] J. Zhang, Y. Yuan, Y. Wang, F. Sun, G. Liang, Z. Jiang, S.-H. Yu, *Nano Res.* **2015**, *8*, 2329.
- [51] S. Wang, X. Meng, A. Das, T. Li, Y. Song, T. Cao, X. Zhu, M. Zhu, R. Jin, *Angew. Chem., Int. Ed.* **2014**, *53*, 2376.
- [52] M. P. Casaletto, A. Longo, A. Martorana, A. Prestianni, A. M. Venezia, *Surf. Interface Anal.* **2006**, *38*, 215.
- [53] J. M. Dixon, S. Egusa, *J. Am. Chem. Soc.* **2018**, *140*, 2265.
- [54] D. M. Chevrier, A. Chatt, P. Zhang, *J. Nanophotonics* **2012**, *6*, 064504.
- [55] M.-C. Bourg, A. Badia, R. B. Lennox, *J. Phys. Chem. B* **2000**, *104*, 6562.
- [56] M. Descostes, F. Mercier, N. Thromat, C. Beaucaire, M. Gautier-Soyer, *Appl. Surf. Sci.* **2000**, *165*, 288.
- [57] Y.-T. Wu, C. Shanmugam, W.-B. Tseng, M.-M. Hiseh, W.-L. Tseng, *Nanoscale* **2016**, *8*, 11210.
- [58] Y. Deng, H. Gruppen, P. A. Wierenga, *J. Agric. Food Chem.* **2018**, *66*, 4219.
- [59] Z. Wu, *Angew. Chem., Int. Ed.* **2012**, *51*, 2934.
- [60] J.-P. Choi, C. A. Fields-Zinna, R. L. Stiles, R. Balasubramanian, A. D. Douglas, M. C. Crowe, R. W. Murray, *J. Phys. Chem. C* **2010**, *114*, 15890.
- [61] H.-W. Li, Y. Yue, T.-Y. Liu, D. Li, Y. Wu, *J. Phys. Chem. C* **2013**, *117*, 16159.
- [62] C. J. Coester, K. Langer, H. Von Briesen, J. Kreuter, *J. Microencapsulation* **2000**, *17*, 187.
- [63] S. A. Khan, M. Schneider, *Macromol. Biosci.* **2014**, *14*, 1627.
- [64] R. Khandelia, S. Bhandari, U. N. Pan, S. S. Ghosh, A. Chattopadhyay, *Small* **2015**, *11*, 4075.
- [65] E. Leo, M. Angela Vandelli, R. Cameroni, F. Forni, *Int. J. Pharm.* **1997**, *155*, 75.
- [66] J. Conde, J. T. Dias, V. Grazú, M. Moros, P. V. Baptista, J. M. de la Fuente, *Front. Chem.* **2014**, *2*, 48.
- [67] S. S. S. Lanke, C. S. Kolli, J. G. Strom, A. K. Banga, *Int. J. Pharm.* **2009**, *365*, 26.
- [68] L. Yang, L. Wu, D. Wu, D. Shi, T. Wang, X. Zhu, *Int. J. Nanomed.* **2017**, *12*, 3357.
- [69] R. M. Hathout, S. Mansour, A. S. Geneidi, N. D. Mortada, *J. Colloid Interface Sci.* **2011**, *354*, 124.
- [70] K. Tomoda, N. Yabuki, H. Terada, K. Makino, *Colloid Polym. Sci.* **2014**, *292*, 3195.
- [71] T. Gratieri, U. F. Schaefer, L. Jing, M. Gao, K. H. Kostka, R. F. Lopez, M. Schneider, *J. Biomed. Nanotechnol.* **2010**, *6*, 586.
- [72] Y. Zou, A. Celli, H. Zhu, A. Elmahdy, Y. Cao, X. Hui, H. Maibach, *Int. J. Nanomed.* **2017**, *12*, 8035.
- [73] T. Zimmermann, *Adv. Biochem. Eng. Biotechnol.* **2005**, *95*, 245.
- [74] F. Stracke, B. Weiss, C.-M. Lehr, K. König, U. F. Schaefer, M. Schneider, *J. Invest. Dermatol.* **2006**, *126*, 2224.
- [75] P. C. DeMuth, W. F. Garcia-Beltran, M. L. Ai-Ling, P. T. Hammond, D. J. Irvine, *Adv. Funct. Mater.* **2013**, *23*, 161.
- [76] J.-Y. Lai, Y.-T. Li, C.-H. Cho, T.-C. Yu, *Int. J. Nanomed.* **2012**, *7*, 1101.
- [77] K. L. Parry, A. G. Shard, R. D. Short, R. G. White, J. D. Whittle, A. Wright, *Surf. Interface Anal.* **2006**, *38*, 1497.
- [78] J. H. Scofield, *J. Electron Spectrosc. Relat. Phenom.* **1976**, *8*, 129.